PHYSICAL REVIEW D **82,** 015001 (2010)

Technicolor corrections to $b\bar{b} \to W^{\pm}\pi_t^{\mp}$ at the CERN Large Hadron Collider

Jinshu Huang*

College of Physics and Electronic Engineering, Nanyang Normal University, Nanyang 473061, People's Republic of China and College of Physics and Information Engineering, Henan Normal University, Xinxiang 453007, People's Republic of China

Qunna Pan† and Taiping Song‡

College of Physics and Electronic Engineering, Nanyang Normal University, Nanyang 473061, People's Republic of China

Gongru Lu§

College of Physics and Information Engineering, Henan Normal University, Xinxiang 453007, People's Republic of China

(Received 2 April 2010; published 1 July 2010)

In this paper we calculate the technicolor correction to the production of a charged top pion in association with a W boson via $b\bar{b}$ annihilation at the CERN Large Hadron Collider in the context of the topcolor assisted technicolor model. We find that the cross section of $pp \to b\bar{b} \to W^{\pm}\pi_t^{\mp}$ at the tree level can reach a few hundred femtobarns for reasonable ranges of the parameters, roughly corresponding to the result of the process $pp \to b\bar{b} \to W^{\pm}H^{\mp}$ in the minimal supersymmetric standard model; the relative corrections arising from the one-loop diagrams are about a few percent to two dozen percent, and they will increase the cross section at the tree level. As a comparison, we also discuss the size of the hadron cross section via the other subprocess $gg \to W^{\pm}\pi_t^{\mp}$.

DOI: 10.1103/PhysRevD.82.015001 PACS numbers: 12.60.Nz, 12.60.Fr, 14.65.Fy

I. INTRODUCTION

Technicolor theory [1,2] is one of the important candidates to probe new physics beyond the standard model (SM), especially the topcolor assisted technicolor (TC2) model proposed by C. T. Hill [3]—it combines technicolor with topcolor, with the former mainly responsible for electroweak symmetry breaking (EWSB) and the latter for generating a major part of the top quark mass. If technicolor is actually responsible for EWSB, there are strong phenomenological arguments that its energy scale is at most a few hundred GeV and that the lightest technicolor pions are within reach of the ATLAS and CMS experiments at the Large Hadron Collider (LHC) [4]. The TC2 model predicts three top pions (π_t^0, $\pi_t^{\pm}$), one top Higgs (h_t^0), and the new gauge bosons (Z', B) with large Yukawa couplings to the third generation quarks, so these new particles can be regarded as a typical feature of this model. Lots of signals of this model have already been studied in the work environment of linear colliders and hadron-hadron colliders [5–7], but most of the attention was focused on the neutral top pion and new gauge bosons. Here we wish to discuss the prospects of charged top pions.

The search for Higgs bosons and new physics particles and the study of their properties are among the prime objectives of the LHC. Recently, lots of studies about the neutral Higgs production at the LHC have been finished [8]. For the production of charged Higgs bosons in association with a W boson in the minimal supersymmetric standard model, Ref. [9] investigates $b\bar{b} \to W^{\pm}H^{\mp}$ at the tree level and $gg \to W^{\pm}H^{\mp}$ at one loop. The electroweak corrections and QCD corrections to $b\bar{b} \to W^{\pm}H^{\mp}$ have already been calculated in Ref. [10], which shows that a favorable scenario for $W^{\pm}H^{\mp}$ associated production would be characterized by the conditions that $m_H > m_t - m_b$ and that $\tan\beta$ are either close to unity or of order m_t/m_b, then the $H^{\pm}$ bosons could not spring from on-shell top quarks and could be so copiously produced at hadron colliders. The authors of Ref. [11] have already studied the process of $W^{\pm}\pi_t^{\mp}$ associated production via $b\bar{b}$ annihilation at the tree level, which shows that the total cross section $\sigma(p\bar{p} \to b\bar{b} \to W^{\pm}\pi_t^{\mp})$ is rather large when $\pi_t^{\pm}$ is not very heavy. In this paper we shall discuss the production of top pions $\pi_t^{\pm}$ in association with SM gauge bosons $W^{\mp}$ including the contributions arising from top pions π_t^0, $\pi_t^{\pm}$ and top Higgs h_t^0, and calculate the total cross section to one-loop order, to search for new physics particles and test the TC2 model.

This paper is organized as follows. Section II is devoted to our analytical results of the cross section of $pp \to b\bar{b} \to W^{\pm}\pi_t^{\mp}$ in terms of the well-known standard notation of one-loop Feynman integrals. The numerical results and conclusions are included in Sec. III.

II. THE CALCULATIONS OF $\sigma(p\bar{p} \to b\bar{b} \to W^{\pm}\pi_t^{\mp})$ AT ONE-LOOP LEVEL

The Feynman diagrams for the charged top pion production via $b(p_1)\bar{b}(p_2) \to W^{\pm}(k_2)\pi_t^{\mp}(k_1)$, which include the technicolor corrections to the process, are shown in Fig. 1. The relevant Feynman rules are given in Refs. [3,12]. In our calculation, we adopt the 't Hooft–Feynman gauge and use the dimensional reduction for

*jshuang@foxmail.com
†qnpan@163.com
‡stp66@sina.com
§lugongru@sina.com

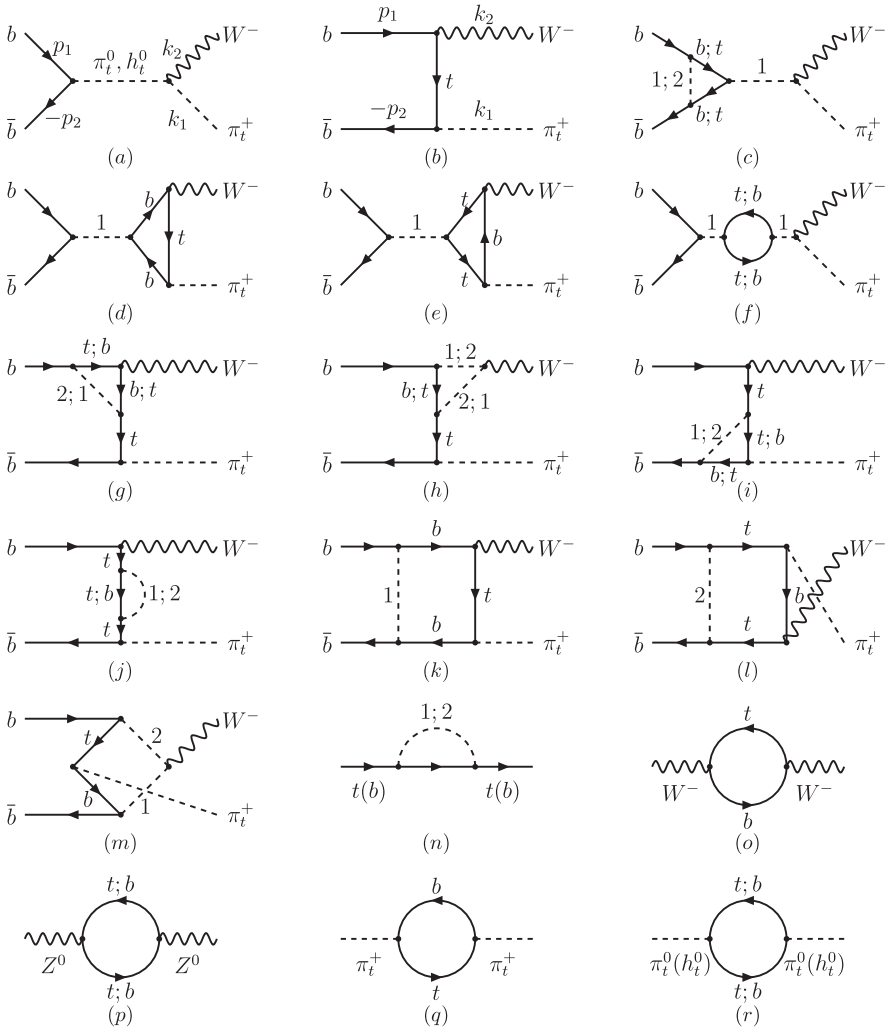

FIG. 1. Feynman diagrams for the technicolor corrections to the $b\bar{b} \to W^- \pi_t^+$ process: (a)–(b) tree-level diagrams; (c)–(m) one-loop diagrams; (n)–(r) the diagrams contributing to renormalization constants. Here the internal dashed line 1 represents the neutral top pion π_t^0 and top Higgs h_t^0, and the dashed line 2 denotes the charged top pion π_t^+.

regularization of the ultraviolet divergences in the virtual loop corrections by the on-mass-shell renormalization scheme [13], in which the fine-structure constant $\alpha_{\rm em}$ and physical masses are chosen to be the renormalized parameters, and finite parts of the counterterms are fixed by the renormalization conditions. The coupling constant g is related to the SM input parameters e, m_W, and m_Z.

The Mandelstam variables are defined as

$$\begin{aligned} \hat{s} &= (p_1 + p_2)^2 = (k_1 + k_2)^2, \\ \hat{t} &= (p_1 - k_2)^2 = (p_2 - k_1)^2, \\ \hat{u} &= (p_1 - k_1)^2 = (p_2 - k_2)^2. \end{aligned} \tag{1}$$

The self-energy coupling between W^+ and π_t^+ has no contribution to their renormalization fields and masses since π_t^+ is a pseudo-Goldstone boson and W^+ is a gauge boson. We follow the approach of A. Mendez and A. Pomarol [14] to define the relevant renormalization constants; the renormalized amplitude for $b\bar{b} \to W^- \pi_t^+$ can be written as

$$M_{\rm rem} = M_0^{(\hat{s})} + M_0^{(\hat{t})} + \delta M, \tag{2}$$

where $M_0^{(\hat{s})}$ and $M_0^{(\hat{t})}$ are the tree-level amplitudes arising from Figs. 1(a) and 1(b), respectively, which are given by

$$\begin{aligned} M_0^{(\hat{s})} = {} & \frac{igm_b(1-\varepsilon)}{\sqrt{2}f_{\pi_t}} \frac{1}{\hat{s} - m_{\pi_t}^2} [\bar{v}(p_2)\gamma_5 u(p_1) \\ & \times (p_1 + p_2)_\mu \varepsilon^\mu(k_2)] - \frac{igm_b(1-\varepsilon)}{\sqrt{2}f_{\pi_t}} \frac{1}{\hat{s} - m_{h_t}^2} \\ & \times [\bar{v}(p_2)u(p_1)(p_1 + p_2)_\mu \varepsilon^\mu(k_2)], \end{aligned} \tag{3}$$

$$\begin{aligned} M_0^{(\hat{t})} = {} & -\frac{ig(1-\varepsilon)}{\sqrt{2}f_{\pi_t}} \frac{1}{\hat{t} - m_t^2} [m_b \bar{v}(p_2)(\not{p}_1 - \not{k}_2) \\ & \times \gamma_\mu L u(p_1)\varepsilon^\mu(k_2) + m_t^2 \bar{v}(p_2)\gamma_\mu L u(p_1)\varepsilon^\mu(k_2)], \end{aligned} \tag{4}$$

and δM denotes all of the one-loop corrections to the tree-level process, which can be represented by

$$\delta M = [\delta\hat{M}^{V_1(\hat{s})} + \delta\hat{M}^{V_2(\hat{s})} + \delta\hat{M}^{S(\hat{s})}](\pi_t^0) + [\delta\hat{M}^{V_1(\hat{s})} + \delta\hat{M}^{V_2(\hat{s})} + \delta\hat{M}^{S(\hat{s})}](h_t^0) + \delta\hat{M}^{V_1(\hat{t})} + \delta\hat{M}^{V_2(\hat{t})} + \delta\hat{M}^{S(\hat{t})} + \delta M^B. \quad (5)$$

The amplitudes $\delta\hat{M}^V$ and $\delta\hat{M}^S$ arising from the self-energy and vertex corrections can be written by

$$\delta\hat{M}^{V_1(\hat{s})}(\pi_t^0) = \frac{igm_b(1-\varepsilon)}{\sqrt{2}f_{\pi_t}}\frac{1}{\hat{s}-m_{\pi_t}^2}\bar{v}(p_2) \times\left[\frac{\delta m_b}{m_b}+\frac{1}{2}\delta Z_L^b+\frac{1}{2}\delta Z_R^b+\frac{1}{2}\delta Z_{\pi_t^0}\right] \times\gamma_5(p_1+p_2)_\mu u(p_1)\varepsilon^\mu(k_2)+\delta M^{V_1(\hat{s})}(\pi_t^0), \quad (6)$$

$$\delta\hat{M}^{V_1(\hat{s})}(h_t^0) = -\frac{igm_b(1-\varepsilon)}{\sqrt{2}f_{\pi_t}}\frac{1}{\hat{s}-m_{h_t}^2}\bar{v}(p_2) \times\left[\frac{\delta m_b}{m_b}+\frac{1}{2}\delta Z_L^b+\frac{1}{2}\delta Z_R^b+\frac{1}{2}\delta Z_{h_t^0}\right] \times(p_1+p_2)_\mu u(p_1)\varepsilon^\mu(k_2)+\delta M^{V_1(\hat{s})}(h_t^0), \quad (7)$$

$$\delta\hat{M}^{V_2(\hat{s})}(\pi_t^0) = \frac{igm_b(1-\varepsilon)}{\sqrt{2}f_{\pi_t}}\frac{1}{\hat{s}-m_{\pi_t}^2}\bar{v}(p_2)\left[\frac{\delta g}{g}+\frac{1}{2}\delta Z_W +\frac{1}{2}\delta Z_{\pi_t^0}+\frac{1}{2}\delta Z_{\pi_t^+}\right]\gamma_5(p_1+p_2)_\mu \times u(p_1)\varepsilon^\mu(k_2)+\delta M^{V_2(\hat{s})}(\pi_t^0), \quad (8)$$

$$\delta\hat{M}^{V_2(\hat{s})}(h_t^0) = -\frac{igm_b(1-\varepsilon)}{\sqrt{2}f_{\pi_t}}\frac{1}{\hat{s}-m_{h_t}^2}\bar{v}(p_2)\left[\frac{\delta g}{g}+\frac{1}{2}\delta Z_W +\frac{1}{2}\delta Z_{h_t^0}+\frac{1}{2}\delta Z_{\pi_t^+}\right](p_1+p_2)_\mu u(p_1)\varepsilon^\mu(k_2) +\delta M^{V_2(\hat{s})}(h_t^0), \quad (9)$$

$$\delta\hat{M}^{S(\hat{s})}(\pi_t^0) = \frac{igm_b(1-\varepsilon)}{\sqrt{2}f_{\pi_t}}\frac{1}{(\hat{s}-m_{\pi_t}^2)^2}\bar{v}(p_2) \times[\delta m_{\pi_t}^2+(m_{\pi_t}^2-\hat{s})\delta Z_{\pi_t^0}]\gamma_5(p_1+p_2)_\mu \times u(p_1)\varepsilon^\mu(k_2)+\delta M^{S(\hat{s})}(\pi_t^0), \quad (10)$$

$$\delta\hat{M}^{S(\hat{s})}(h_t^0) = -\frac{igm_b(1-\varepsilon)}{\sqrt{2}f_{\pi_t}}\frac{1}{(\hat{s}-m_{h_t}^2)^2}\bar{v}(p_2) \times[\delta m_{h_t}^2+(m_{h_t}^2-\hat{s})\delta Z_{h_t^0}](p_1+p_2)_\mu \times u(p_1)\varepsilon^\mu(k_2)+\delta M^{S(\hat{s})}(h_t^0), \quad (11)$$

$$\delta\hat{M}^{V_1(\hat{t})} = -\frac{ig(1-\varepsilon)}{\sqrt{2}f_{\pi_t}}\frac{1}{\hat{t}-m_t^2}\Big[m_b\bar{v}(p_2)\Big(\frac{\delta g}{g}+\frac{1}{2}\delta Z_L^t +\frac{1}{2}\delta Z_L^b+\frac{1}{2}\delta Z_W\Big)(\not{p}_1-\not{k}_2)\gamma_\mu Lu(p_1)\varepsilon^\mu(k_2) +m_t^2\bar{v}(p_2)\Big(\frac{\delta g}{g}+\frac{1}{2}\delta Z_L^t+\frac{1}{2}\delta Z_L^b+\frac{1}{2}\delta Z_W\Big) \times\gamma_\mu Lu(p_1)\varepsilon^\mu(k_2)\Big]+\delta M^{V_1(\hat{t})}, \quad (12)$$

$$\delta\hat{M}^{V_2(\hat{t})} = -\frac{ig(1-\varepsilon)}{\sqrt{2}f_{\pi_t}}\frac{1}{\hat{t}-m_t^2}\Big[m_b\bar{v}(p_2)\Big(\frac{\delta m_b}{m_b}+\frac{1}{2}\delta Z_R^b +\frac{1}{2}\delta Z_L^t+\frac{1}{2}\delta Z_{\pi_t^+}\Big)(\not{p}_1-\not{k}_2)\gamma_\mu Lu(p_1)\varepsilon^\mu(k_2) +m_t^2\bar{v}(p_2)\Big(\frac{\delta m_t}{m_t}+\frac{1}{2}\delta Z_L^b+\frac{1}{2}\delta Z_R^t+\frac{1}{2}\delta Z_{\pi_t^+}\Big) \times\gamma_\mu Lu(p_1)\varepsilon^\mu(k_2)\Big]+\delta M^{V_2(\hat{t})}, \quad (13)$$

$$\delta\hat{M}^{S(\hat{t})} = \frac{ig(1-\varepsilon)}{\sqrt{2}f_{\pi_t}}\frac{1}{(\hat{t}-m_t^2)^2}\Big[m_b\bar{v}(p_2)\delta Z_L^t(\not{p}_1-\not{k}_2)(\not{p}_1-\not{k}_2)(\not{p}_1-\not{k}_2)\gamma_\mu Lu(p_1)\varepsilon^\mu(k_2)+\bar{v}(p_2)\Big(\frac{1}{2}m_t^2\delta Z_L^t+\frac{1}{2}m_t^2\delta Z_R^t -m_t\delta m_t\Big)(\not{p}_1-\not{k}_2)(\not{p}_1-\not{k}_2)\gamma_\mu Lu(p_1)\varepsilon^\mu(k_2)+\bar{v}(p_2)(m_t^2(m_t-m_b)\delta Z_R^t-m_bm_t^2\delta Z_L^t-2m_bm_t\delta m_t) \times(\not{p}_1-\not{k}_2)\gamma_\mu Lu(p_1)\varepsilon^\mu(k_2)-m_t^3\bar{v}(p_2)\Big(\frac{1}{2}m_t\delta Z_L^t+\frac{1}{2}m_t\delta Z_R^t+\delta m_t\Big)\gamma_\mu Lu(p_1)\varepsilon^\mu(k_2)\Big]+\delta M^{S(\hat{t})}. \quad (14)$$

The one-loop amplitudes $\delta M^{V_1(\hat{s})}(\pi_t^0)$, $\delta M^{V_2(\hat{s})}(\pi_t^0)$, $\delta M^{S(\hat{s})}(\pi_t^0)$, $\delta M^{V_1(\hat{s})}(h_t^0)$, $\delta M^{V_2(\hat{s})}(h_t^0)$, $\delta M^{S(\hat{s})}(h_t^0)$, $\delta M^{V_1(\hat{t})}$, $\delta M^{V_2(\hat{t})}$, $\delta M^{S(\hat{t})}$, and δM^B represent the irreducible corrections arising, respectively, from the $b\bar{b}\pi_t^0$ vertex diagram shown in Fig. 1(c), the $W^-\pi_t^+\pi_t^0$ vertex diagrams in Figs. 1(d) and 1(e), the π_t^0 self-energy diagram in Fig. 1(f), the $b\bar{b}h_t^0$ vertex diagram in Fig. 1(c), the $W^-\pi_t^+h_t^0$ vertex diagrams in Figs. 1(d) and 1(e), the h_t^0 self-energy diagram in Fig. 1(f), the btW^- vertex diagrams in Figs. 1(g) and 1(h), the $t\bar{b}\pi_t^+$ vertex diagrams in

Fig. 1(i), the top quark self-energy diagram in Fig. 1(j), and the box diagrams in Figs. 1(k)–1(m).

Calculating the self-energy diagrams in Figs. 1(n)–1(r), we can get the expressions of all the renormalization constants.

The detailed expressions of all above δM^V, δM^S, and δM^B and the renormalization constants are tedious, so we do not present them here.

The corresponding amplitude squared is

$$\bar{\sum}|M_{\rm ren}|^2 = \bar{\sum}|M_0^{(\hat{s})} + M_0^{(\hat{t})}|^2 + 2{\rm Re}\bar{\sum}[\delta M(M_0^{(\hat{s})} + M_0^{(\hat{t})})^\dagger]. \tag{15}$$

The cross section for the process $b\bar{b} \to W^\pm \pi_t^\mp$ is

$$\hat{\sigma} = \int_{\hat{t}_-}^{\hat{t}_+} \frac{1}{16\pi\hat{s}^2}\bar{\sum}|M_{\rm ren}|^2 d\hat{t}, \tag{16}$$

with

$$\hat{t}_\pm = \frac{m_W^2 + m_{\pi_t}^2 - \hat{s}}{2} \pm \frac{1}{2} \times \sqrt{[\hat{s} - (m_W + m_{\pi_t})^2][\hat{s} - (m_W - m_{\pi_t})^2]}. \tag{17}$$

The total hadronic cross section for $pp \to b\bar{b} \to W^\pm \pi_t^\mp$ can be obtained by folding the subprocess cross section $\hat{\sigma}$ with the parton luminosity [9]

$$\sigma(s) = \int_{(m_W + m_{\pi_t})/\sqrt{s}}^1 dz \frac{dL}{dz}\hat{\sigma}(b\bar{b} \to W^\pm \pi_t^\mp \quad \text{at } \hat{s} = z^2 s). \tag{18}$$

Here $\sqrt{s}$ and $\sqrt{\hat{s}}$ are the center-of-mass energies of the pp and $b\bar{b}$ states, respectively, and dL/dz is the parton luminosity, defined as [9,10]

$$\frac{dL}{dz} = 2z\int_{z^2}^1 \frac{dx}{x} f_{b/p}(x,\mu) f_{\bar{b}/p}(z^2/x,\mu), \tag{19}$$

where $f_{b/p}(x,\mu)$ and $f_{\bar{b}/p}(z^2/x,\mu)$ are the bottom quark and bottom antiquark parton distribution functions, respectively.

III. NUMERICAL RESULTS AND CONCLUSIONS

We are now in a position to explore the phenomenological implications of our results. The SM input parameters for our numerical analysis are $G_F = 1.16639 \times 10^{-5}$ GeV^{-2}, $m_W = 80.398$ GeV, $m_Z = 91.1876$ GeV, $m_t = 171.2$ GeV, and $m_b = 4.2$ GeV [15]. We use LOOPTOOLS [16] and the CTEQ6M parton distribution function [17] with $\mu = \sqrt{s}/2$. The parameter ε and the masses of top pion π_t^0, $\pi_t^\pm$ and top Higgs h_t^0 are all model-dependent [3], we select them as free parameters, and take

$$0.03 \le \varepsilon \le 0.1, \qquad 200\ {\rm GeV} \le m_{\pi_t} \le 600\ {\rm GeV}, \tag{20}$$

and $m_{h_t} = 150, 250$ GeV to estimate the total cross section of $W^\pm \pi_t^\mp$ associated production at the LHC. We sum over the final states $W^+\pi_t^-$ and $W^-\pi_t^+$ considering their symmetry.

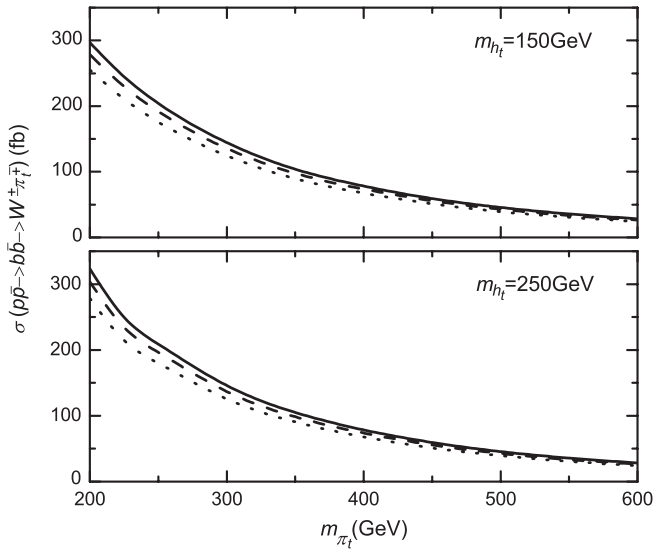

FIG. 2. The total cross section $\sigma(pp \to b\bar{b} \to W^\pm \pi_t^\mp)$ at the tree level versus m_{π_t} for $\varepsilon = 0.03$ (solid line), 0.06 (dashed line), and 0.1 (dotted line).

The final numerical results are summarized in Figs. 2–5. In Fig. 2, the total cross section $\sigma(pp \to b\bar{b} \to W^\pm \pi_t^\mp)$ at the tree level as a function of m_{π_t} for $m_{h_t} = 150, 250$ GeV at the LHC with $L = 100$ fb^{-1} is given, in which the solid lines, dashed lines, and dotted lines denote, respectively, the cases of $\varepsilon = 0.03$, 0.06, and 0.1. From this diagram, we can see that (i) the total cross section decreases quickly as m_{π_t} increase, meanwhile, it changes the values from 2.79×10^2 fb to 26.6 fb with the range of m_{π_t}, $200 \sim 600$ GeV for $\varepsilon = 0.06$ and $m_{h_t} = 150$ GeV, and from 3.04×10^2 fb to 26.6 fb for $\varepsilon = 0.06$ and $m_{h_t} = 250$ GeV, respectively; (ii) the cross section is sensitive to ε and m_{h_t} when m_{π_t} is small, but this sensitivity will disappear for a rather heavy top pion; and (iii) when $m_{\pi_t} = 225$ GeV, the cross section of $W^\pm \pi_t^\mp$ associated production via $b\bar{b}$ annihilation is roughly 250 fb, and is rather large.

Figure 3 gives the plots of the fully integrated cross section via $b\bar{b}$ annihilation at the tree level versus ε for $m_{\pi_t} = 225, 350$, and 450 GeV. We can observe that (i) the cross section is not sensitive to ε, and only decreases by $13.6\% \sim 14.2\%$ in the range of $0.03 \le \varepsilon \le 0.1$ for $m_{h_t} = 150$ GeV; and (ii) the case of $m_{h_t} = 250$ GeV is almost the same as that of $m_{h_t} = 150$ GeV.

In order to look at the contributions of the one-loop Feynman diagrams, we plot the relative correction $\delta\sigma/\sigma_0$ as a function of m_{π_t} and ε in Figs. 4 and 5, in which σ_0 denotes the corresponding total cross section at the tree level. From these two diagrams, we can find that (i) for the case of $m_{h_t} = 150$ GeV, the relative correction

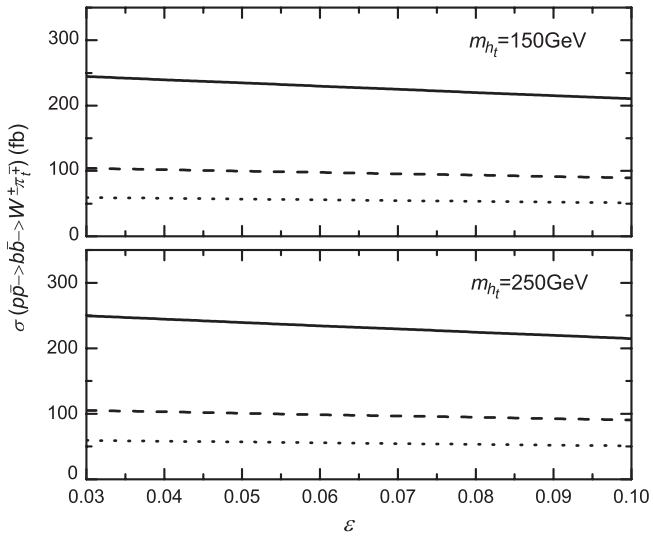

FIG. 3. The curve of $\sigma(pp \to b\bar{b} \to W^{\pm}\pi_t^{\mp})$ at the tree level versus ε for $m_{\pi_t} = 225$ GeV (solid line), 350 GeV (dashed line), and 450 GeV (dotted line).

$\delta\sigma/\sigma_0$ is positive, and decreases with the increases of m_{π_t} and ε, but this decrease is rapid with m_{π_t} and is slow with ε at the changing from 0.03 to 0.1; (ii) for the case of $m_{h_t} = 250$ GeV, the relative correction is slightly larger than that of $m_{h_t} = 150$ GeV; and (iii) the value of the relative correction, in general, is about a few percent to two dozen percent—this means that the contribution from the one-loop corrections can afford a more distinct change than that of the tree level.

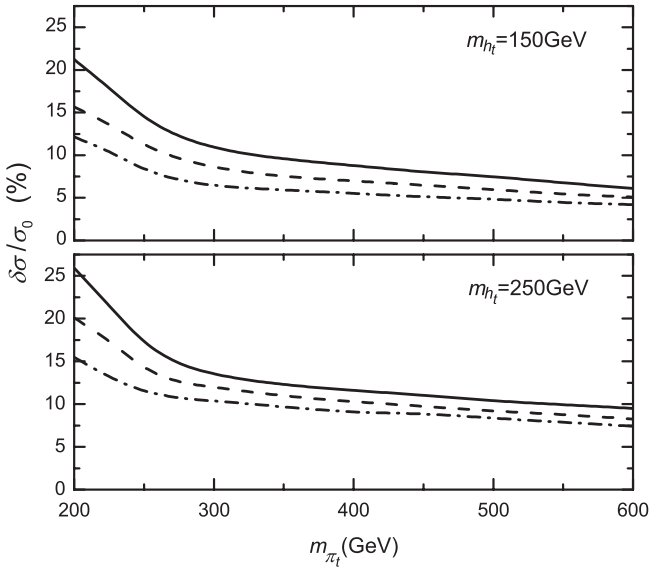

FIG. 4. The relative correction to the cross section $\delta\sigma/\sigma_0$ as a function of m_{π_t} with $m_{h_t} = 150, 250$ GeV and $\varepsilon = 0.03$ (solid line), 0.06 (dashed line), and 0.1 (dot-dashed line).

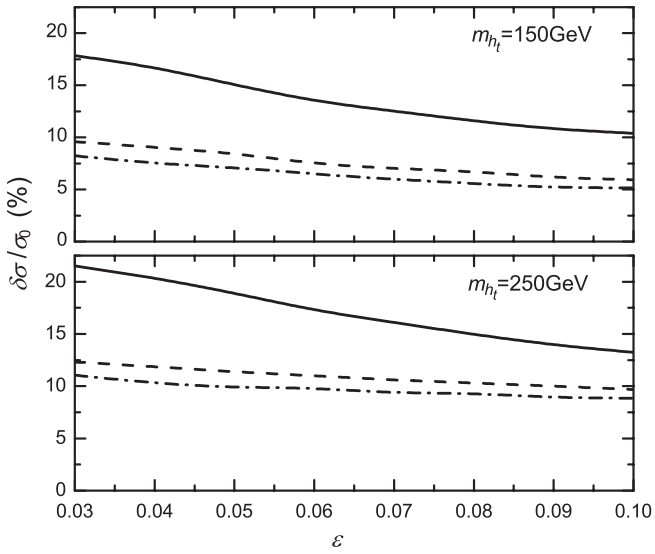

FIG. 5. The relative correction versus ε for $m_{\pi_t} = 225$ GeV (solid line), 350 GeV (dashed line), and 450 GeV (dot-dashed line), respectively.

As is known, at the LHC, the integrated luminosity is expected to reach $L = 100$ fb^{-1} per year; this shows that a cross section of 1 fb could translate into about 60 detectable $W^{\pm}H^{\mp}$ events per year [9,15]. Looking at Figs. 2 and 3, we thus conclude that, if $m_{\pi_t} = 225$ GeV, depending on ε, one should be able to collect an annual total of between 1.26×10^4 and 1.5×10^4 events. So the $W^{\pm}\pi_t^{\mp}$ signal should be clearly visible at LHC unless m_{π_t} is very large. Moreover, the total cross section will enhance a few percent to two dozen percent, arising from the one-loop technicolor corrections.

We know there are mainly two parton subprocesses that contribute to the hadronic cross section $pp \to W^{\pm}\pi_t^{\mp}$: the $b\bar{b}$ annihilation and the gg fusion. In this paper, we only focus on the discussion of the $b\bar{b}$ annihilation. For the gg fusion, there is no tree-level contribution to the subprocess $gg \to W^{\pm}\pi_t^{\mp}$ in the TC2 model, however, at the one-loop level, the process $gg \to W^{\pm}\pi_t^{\mp}$ can be induced by quark-loop diagrams including the triangle diagrams and the box diagrams. Calculating the contributions of these diagrams, we can find that the cross section of $pp \to gg \to W^{\pm}\pi_t^{\mp}$ is between 11.3 and 82.6 fb for reasonable ranges of the parameters, and the changes of $\sigma(pp \to gg \to W^{\pm}\pi_t^{\mp})$ with the parameters m_{π_t}, m_{h_t}, and ε are very similar to those of $b\bar{b}$ annihilation at the tree level given in the Figs. 2 and 3. Whereas the production cross section based on $gg \to W^{\pm}\pi_t^{\mp}$ can be comparable to that via $b\bar{b} \to W^{\pm}\pi_t^{\mp}$ due to the large number of gluons in the high energy proton beams at the LHC. The total cross section of $W^{\pm}\pi_t^{\mp}$ associated production at the LHC should be the sum over these two parton subprocesses.

In conclusion, we have calculated the technicolor corrections to the cross section for $W^{\pm}\pi_t^{\mp}$ associated produc-

tion via $b\bar{b}$ annihilation at the CERN LHC in the topcolor assisted technicolor model. We find that the total cross section of $pp \to b\bar{b} \to W^{\pm}\pi_t^{\mp}$ at the tree level is roughly corresponding to that of the process $pp \to b\bar{b} \to W^{\pm}H^{\mp}$ in the minimal supersymmetric standard model, and can reach a few hundred femtobarns with reasonable values of the parameters. Considering the technicolor corrections arising from the one-loop diagrams, the relative correction is about a few percent to two dozen percent. The size of the cross section via the subprocess $gg \to W^{\pm}\pi_t^{\mp}$ is calculated. Thus, it is so large that the signal of charged top pion should be clearly visible at LHC.

ACKNOWLEDGMENTS

This project was supported in part by the National Natural Science Foundation of China under Grant Nos. 10975047 and 10979008; the Natural Science Foundation of Henan Province under Nos. 092300410205 and 102300410210.

[1] S. Weinberg, Phys. Rev. D **13**, 974 (1976); **19**, 1277 (1979); L. Susskind, *ibid.* **20**, 2619 (1979).
[2] S. Dimopoulos and L. Susskind, Nucl. Phys. **B155**, 237 (1979); E. Eichten and K. Lane, Phys. Lett. **90B**, 125 (1980); E. Farhi and L. Susskind, Phys. Rep. **74**, 277 (1981); J. Ellis, M. K. Gaillard, D. V. Nanopoulos, and P. Sikivie, Nucl. Phys. **B182**, 529 (1981).
[3] C. T. Hill, Phys. Lett. B **345**, 483 (1995); K. Lane, *ibid.* **357**, 624 (1995); C. T. Hill and E. H. Simmons, Phys. Rep. **381**, 235 (2003).
[4] M. Carena, T. Han, G. Y. Huang, and C. E. M. Wagner, J. High Energy Phys. 04 (2008) 092; G. Aad *et al.* (ATLAS Collaboration), arXiv:0901.0512.
[5] X. L. Wang, Y. L. Yang, B. Z. Li, C. X. Yue, and J. Y. Zhang, Phys. Rev. D **66**, 075009 (2002); X. L. Wang and X. X. Wang, *ibid.* **72**, 095012 (2005); J. S. Huang and G. R. Lu, *ibid.* **78**, 035007 (2008).
[6] C. X. Yue, H. J. Zong, and S. Z. Wang, Phys. Lett. B **575**, 25 (2003); C. X. Yue and L. N. Wang, J. Phys. G **34**, 139 (2007); C. X. Yue, Z. J. Zong, L. L. Xu, and J. X. Chen, Phys. Rev. D **73**, 015006 (2006).
[7] J. J. Cao, Z. H. Xiong, and J. M. Yang, Phys. Rev. D **67**, 071701(R) (2003); J. J. Cao, G. L. Liu, and J. M. Yang, *ibid.* **70**, 114035 (2004); Eur. Phys. J. C **41**, 381 (2005).
[8] K. Jakobs, Eur. Phys. J. C **59**, 463 (2009); D. de Florian and M. Grazzini, Phys. Lett. B **674**, 291 (2009).
[9] D. A. Dicus, J. L. Hewett, C. Kao, and T. G. Rizzo, Phys. Rev. D **40**, 787 (1989); A. A. Barrientos Bendezu and B. A. Kniehl, *ibid.* **59**, 015009 (1998); **61**, 097701 (2000); O. Brein, W. Hollik, and S. Kanemura, *ibid.* **63**, 095001 (2001); D. Eriksson, S. Hesselbach, and J. Rathsman, Eur. Phys. J. C **53**, 267 (2008).
[10] Y. S. Yang, C. S. Li, L. G. Jin, and S. H. Zhu, Phys. Rev. D **62**, 095012 (2000); W. Hollik and S. H. Zhu, *ibid.* **65**, 075015 (2002); E. Asakawa, O. Brein, and S. Kanemura, *ibid.* **72**, 055017 (2005); J. Zhao, C. S. Li, and Q. Li, *ibid.* **72**, 114008 (2005); J. Gao, C. S. Li, and Z. Li, *ibid.* **77**, 014032 (2008).
[11] J. S. Huang and Q. N. Pan, Commun. Theor. Phys. **42**, 573 (2004).
[12] R. K. Kaul, Rev. Mod. Phys. **55**, 449 (1983); E. Eichten, I. Hinchliffe, K. Lane, and C. Quigg, Rev. Mod. Phys. **56**, 579 (1984); V. A. Miransky, M. Tanabashi, and K. Yamawaki, Phys. Lett. B **221**, 177 (1989); W. A. Bardeen, C. T. Hill, and M. Lindner, Phys. Rev. D **41**, 1647 (1990); C. T. Hill, D. Kennedy, T. Onogi, and H. L. Yu, *ibid.* **47**, 2940 (1993); V. Labicz, Nucl. Phys. **B404**, 559 (1993); G. Burdman, Phys. Rev. Lett. **83**, 2888 (1999).
[13] M. Bohm, H. Spiesberger, and W. Hollik, Fortschr. Phys. **34**, 687 (1986); W. Hollik, *ibid.* **38**, 165 (1990); B. Grzadkowski and W. Hollik, Nucl. Phys. **B384**, 101 (1992).
[14] A. Mendez and A. Pomarol, Phys. Lett. B **279**, 98 (1992).
[15] C. Amsler *et al.* (Particle Data Group), Phys. Lett. B **667**, 1 (2008).
[16] T. Hahn and M. Perez-Victoria, Comput. Phys. Commun. **118**, 153 (1999); T. Hahn, Acta Phys. Pol. B **30**, 3469 (1999); Nucl. Phys. B, Proc. Suppl. **89**, 231 (2000).
[17] J. Pumplin, A. Belyaev, J. Huston, D. Stump, and W. K. Tung, J. High Energy Phys. 02 (2006) 032.